

Nonclassical light from large ensemble of trapped ions

P. Obšil¹, L. Lachman¹, T. Pham², A. Lešundák², V. Hucl²,
M. Čížek², J. Hrabina², O. Číp², L. Slodička¹ and R. Filip¹

¹ *Department of Optics, Palacký University, 17. listopadu 12, 771 46 Olomouc, Czech Republic*

² *Institute of Scientific Instruments of the Czech Academy of Sciences,
Královopolská 147, 612 64 Brno, Czech Republic*

(Dated: December 14, 2024)

The waste majority of physical objects we are dealing with is almost exclusively made of fundamental constituents of matter - atoms. At the same time, atoms have proved to be emitters of light field which is incompatible with classical description of electromagnetic waves [1]. This peculiar property is intrinsic consequence of an atom being a fundamental physical unit incapable of simultaneous emission of more than one photon. We experimentally demonstrate that the observability of quantumness of atomic fluorescence can be naturally preserved when scaling up the size of the atomic ensemble by several orders of magnitude. Presented measurements of light unconditionally emitted from ionic ensembles of up to more than thousand ions promise early construction of truly macroscopic and intensive sources of quantum light and substantially shift the range of energies in which observable manifestations of discrete quantum features of light and matter should be anticipated.

PACS numbers:

In 1905 Albert Einstein discovered that light can be understood as a stream of interfering photons [2]. At that time it was a contradiction to Maxwell theory of light waves [3]. Quantum optics, however, merges understanding of both wave and particle aspects together [4]. It seems to be expectable that light produced by large number of emitters is commonly considered to be a mixture of classical waves [5]. This has been certified by number of experiments analyzing various light sources from sun-light to laser radiation even with arbitrary small intensity [6]. On the other hand, light from a single emitter with a transition between two energy levels of atom or solid-state object is always nonclassical. Detection of individual photon emitted from single emitter cannot be described by a mixture of classical waves and therefore many results of single-photon experiments contradict classical coherence theory [7]. The most basic contradiction is observation of indivisibility of single photon at a beam splitter, which does not happen for classical light waves [8, 9]. However, it is already different for two photons as they can be split by linear optics. It is evident that ideal particle indivisibility is lost for large number of photons even though some particle-type nonclassical features may remain. It is intuitively clear that a state of a finite number of photons cannot be modelled as a mixture of classical waves, as those are always based on distribution of photons up to infinity. This particle-type of nonclassicality can remain hidden since the limitation in number of photons can be far away from what is detectable, as can be seen on classical sources consisting of enormous amount of quantum emitters.

Observability of truly particle aspects of light therefore typically vanishes in everyday macroscopic reality and we frequently observe only mixtures of classical waves. It is due to inevitable enhancement of effects which deteriorate the macroscopic photon samples, but also affect their

macroscopic sources and detectors. However, those effects are not fundamental and macroscopicity itself does not smudge the particle features. In order to succeed with detection of particle nonclassical aspects of light for large number quantum emitters the employed detection setup and evaluation procedure must provide unambiguous identification and sufficient information about nonclassical light without any prior assumptions. In addition, the measured light source needs to be stable in the number of photon emitters and the collection efficiency of unconditionally emitted light by detector has to be sufficiently high to overcome the effects of background thermal noise. The detection apparatus and the employed criterion should be able to detect nonclassicality for large number of photons in the presence of high loss, finite amplitude of added thermal noise and within feasible measurement times. These requirements have long forced the particle nonclassicality of radiation from large ensembles of emitters and its possible applications to remain in the domain of theoretical considerations. Up to few notable recent stimuli, which provide substantial evidence that nonclassicality is not necessarily bound to a few emitters [10, 11], experimental observations have been concerned by the analysis and control of nonclassical features on very small number of emitters. The ingenious fundamental questions considering the limits on the size of the particle samples and its number statistics, applicability of possible nonclassicality in large ensembles for detection of related fundamental effects like quantum phase transitions, particle entanglement, or its possible utilization for mesoscopic quantum computation still remain to be explored.

Ensemble of large number of ions trapped in a Paul trap possesses several crucial advantages for initial proof-of-principle tests of nonclassicality [12]. First, average trapping lifetimes of single ions in our setup are exceed-

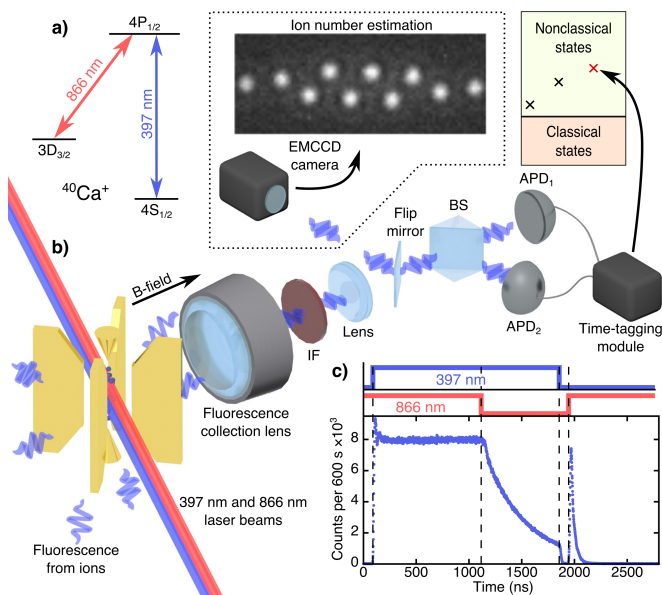


FIG. 1: The simplified scheme of experimental setup and laser pulse sequence for generation and detection of nonclassical light. a) The energy level scheme of the $^{40}\text{Ca}^+$ ion including employed transitions with their respective wavelengths. b) An ensemble of ions is trapped in the linear Paul trap and the 397 nm fluorescence emitted along the applied magnetic field direction (B-field) is collected by lens objective and separated from the 866 nm light by optical interference filter (IF). The fluorescence is then directed towards nonclassicality analyzing setup comprising single beam-splitter (BS), a pair of avalanche photodiodes (APDs) and the time-tagging module. The trapped ion crystals can be imaged on EMCCD camera for the purposes of ion number estimation and optimization of trapping stability. c) The generation of analyzed light from trapped ion ensemble in pulsed regime begins by Doppler cooling period, in which both lasers are switched on. It is followed by the optical pumping stage, where the populations are shuffled to the metastable $3D_{3/2}$ state by shining in only the 397 nm laser. The analyzed fluorescence at $4P_{1/2} \leftrightarrow 4S_{1/2}$ transition is then generated by fast depopulation of the $3D_{3/2}$ state using the 866 nm laser pulse.

ing several days what allows for direct observation of nonclassicality even for very large ion numbers [13]. Second, laser cooled and trapped ion crystals can correspond to isotopically pure samples of ions with lambda-type electronic level scheme and similar setups have been recently used for demonstration of single-photon sources with record-breaking purity [14–17]. Furthermore, the typical inter-atomic distance of ions in the traps is limited to be much larger than the wavelengths of the involved optical transitions due to the Coulomb repulsion, what suggest, that spontaneous build-up of collective effects can be neglected and ions can be treated as mutually independent emitters [18]. In addition, ion trapping apparatus allows for near perfect control of number of emitters in the crystal due to albeit probabilistic, however easily repeatable ion-loading procedures.

In our measurements we focus on reaching the maximal number of participating ions while still unambiguously demonstrating the nonclassicality of the emitted light field allowed by practical limits related to the ion trapping and light collection apparatus. The simplified scheme of our experimental setup is shown in Fig. 1. The $^{40}\text{Ca}^+$ ion crystal is created by application of the trapping and Doppler-cooling forces in the potential minimum of a linear Paul trap. The light scattered from ions is collected using lens covering $\approx 2\%$ of the full solid angle with radial position and focal point carefully optimized for maximizing the fluorescence detection efficiency from single ion trapped in the trap center, see Supplementary material A for more experimental details.

Nonclassical features of atomic fluorescence coming from trapped ion crystals are estimated by statistical analysis of the recorded time-tagged detection signal corresponding to exact times of photon arrivals at the two avalanche photodiodes (APDs) using the criteria from Lachman et al. [12]. Differently to criteria that incorporate moments of photon distribution [19, 20], this criterion includes real response of employed single-photon detectors and takes into account possible unequal quantum detection efficiencies. It thus allows for unambiguous test of nonclassicality of light even with high mean number of photons. The nonclassicality is then witnessed by estimation of probabilities of detecting no photon on both detectors P_{00} and detecting no photon on one particular detector P_0 within given time bin period and evaluation of the distance from the nonclassicality threshold defined as

$$d = P_0 - \sqrt{P_{00}} > 0. \quad (1)$$

We measure the statistics of emitted fluorescence in both pulsed and continuous excitation regimes, which effectively represent different sources of radiation. In the continuous case, ions in the crystal emit fluorescence at random and mutually uncorrelated times and in principle, finite linewidth of the employed transition and laser light leakage can result in multiple emissions from single ion within the same time bin. This is well illustrated by the decreased purity of the emitted single photons from single atoms in continuous schemes compared to pulsed sources, in which the multiphoton emission is typically prohibited by optical pumping mechanism [14–17]. The pulsed driving is thus much more convenient for demonstration of the nonclassical emission from large atomic ensembles, provided that the rate of the photon emission given by pulse sequence length can be kept comparably high. As can be seen in Fig. 1-a) and 1-c), we employ an effectively three-level energy structure of the $^{40}\text{Ca}^+$ to minimize the multiphoton content in the given measurement time-bin by optically pumping the atomic population to the to the metastable $3D_{3/2}$ level from where the photon emission is initiated by 866 nm laser pulse. The optical pumping characteristic time is relatively long for our excitation parameters and crystal spatial extensions and depending on the laser settings, about one fifth of

emitters remains in the $4S_{1/2}$ level. The single photon detectors are gated with the gating time optimized to comprise most of the generated 397 nm light. The detailed description of measured data processing can be found in Supplementary material B.

The evaluated difference d (1) for trapped ion crystals containing from one to up to several hundreds of ions is plotted in Fig. 2-a). A clear violation of the nonclassicality condition is observed for number of ions reaching 275 in both continuous and pulsed regimes. The corresponding theoretical prediction of parameter d in the pulsed regime has been evaluated and plotted by taking into account distribution of detection efficiencies for ions in the given crystal. The theoretical prediction agrees well with the measured data, even without any free fitting parameter and without taking into account experimental imperfections like the optical pumping spatial distribution, or intensity fluctuations of exciting lasers. In the presented simulation, we have considered the ion crystals with concentric shell structure supported by our observations. Details of the simulation can be found in Supplementary material C. The ion storage lifetime and crystal stability can play a crucial role for the statistical properties of the emitted light. We have analyzed the rate of loss of ions in our setup in the regime where cooling lasers frequencies are locked and trap input RF power remains stable. Number of trapped ions has been precisely counted before and after each photon-counting measurements and there has been no observable loss of ions in the presented measurements. We note, that only 2 out of 14 measurement runs were discarded due to loss of ions caused by cooling laser frequency instability.

The internal atomic dynamics and multi-photon contributions make it difficult to theoretically predict the measured parameter d in continuous regime. The actual uncertainty in the emission time and possibility of multiphoton contributions from single atoms within finite time bins make this regime closer to large class of optical sources with uncontrolled internal dynamics or partial coupling to environment [21] and presented measurements will likely stimulate investigations of their statistical properties.

The technical limit on further increase of number of emitters in our experiment is given by the effective detection volume of the employed optical detection setup. The photon detection efficiency falls rapidly for ions positioned in the radial direction from the collection lens focal point and less rapidly, but still considerably, along the lens symmetry axis, see Supplementary information A for more details. The limiting radial size of the detection volume for our detection arrangement is $4.6 \mu\text{m}$ (FWHM). The detection efficiency variation at various distances from the lens focal point suggests that increase of the measured crystal size beyond hundreds of ions in our setup inevitably places some of them into regions with extremely small relative collection efficiency. The transition to small relative detection efficiencies is smooth in all three spatial directions, which brings in a

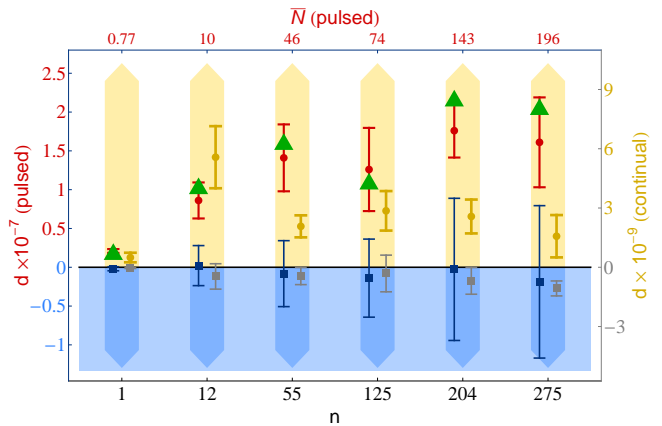


FIG. 2: The measured violation of nonclassicality as the function of number of trapped single photon emitters and the same measurements realized just with the laser light. All measured distances d for trapped ion ensembles in pulsed (red circles) and continuous (yellow circles) regimes are provably in the nonclassical region given by the positive distance d . The green triangles correspond to the numerical simulation of the distance in the pulsed regime. The distance d for the 397 nm laser light scattered from the trap electrodes has been measured using the same detection scheme in both excitation regimes for mean photon numbers \bar{N} set to the value corresponding to the measured photon flux from the trapped ion ensemble. The dark blue and grey squares are measurements on the laser light in the pulsed and continuous regimes, respectively. Error bars correspond to one standard deviation for all displayed data points.

technical question of how many emitters actually substantially contribute to detected photon flux. This fuzziness in the number of contributing emitters is seen as an actual sign of dealing with a system which approaches the fragile borderline between the applicability of quantum and classical descriptions, at which the suitability of the discrete quantum description of some important physical variables, like number of emitters or total energy, naturally deteriorates. The mere technical limit of the employed optical detection setup can be eliminated by the use of optimized imaging configuration. We demonstrate further scalability of the nonclassicality measurements in similar setups by changing the lens configuration so that we decrease its overall magnification factor, which corresponds to an increase of the radial detection volume. We reach the radial field of view $9.6 \mu\text{m}$ without observing any substantial change of the absolute detection efficiency of ion positioned on the optical axis. With this configuration, we have measured the positive distance $d = (9.48 \pm 3.93) \times 10^{-7}$ for 1500 ± 200 ions in equal 5 hour long experimental run.

The photon flux at the input of the detection apparatus has been estimated for each measurement in the pulsed regime from the number of trapped emitters and measured finite efficiency of the optical pumping. The highest mean photon number at the input of our detec-

tion apparatus is $\bar{N} = 196$ photons, which correspond to $n = 275$ ions and 71% optical pumping efficiency. To the best of our knowledge, that corresponds both to the largest ensemble of single photon emitters and largest photonic field for which nonclassical statistical properties have been demonstrated. Furthermore, as can be seen in Fig. 2-a), the relative uncertainty of the measurements of the distance d scales very favorably with number of ions, which promises scalability of our measurements to much higher ion numbers, provided that the emitted light will be collected efficiently.

Furthermore, there seems to be no fundamental limit on further substantial increase of any of these quantities in the similar experimental apparatus. We have simulated the emission of light from crystal containing up to 10^5 ions. The simulation predicts scaling of the parameter d and uncertainty caused by finite measurement with size of the crystal. As already predicted in Ref. [12], the main limiting parameter for unambiguous detection of nonclassicality for stable ensemble of single photon emitters is the measurement time. The detailed analysis presented in Supplementary materials C shows, that the required experimental time does not grow substantially until the mean photon flux at detectors reaches several photons. The nonclassicality of stronger light would be also observable, however it would require additional attenuation to reach the optimal photon flux for measuring

nonclassical properties.

Presented measurements demonstrate the first unambiguous proof of nonclassical character of light field emitted from large ensemble of single photon emitters. We have shown that ensembles consisting of emitters which individually produce nonclassical light, keep this statistical property when scaling up their size by at least two orders of magnitude. Moreover, the demonstrated nonclassicality measurements present robustness against many imperfections of individual sources. We have also verified several aspects of emission from ensemble of single-photon-sources compared to emission from a single one. Most notably that the measured nonclassicality witness value grows with the increasing emitter number. Our experimental test opens possibilities of search for nonclassical light emission from recently developed ensembles of atomic [22, 23] and solid-state emitters [10, 11] and study their internal dynamics from a new perspective [24–26]. It will allow their exploration before single emitters are isolated and further direct exploitation in quantum technology. Our demonstration can be directly extended in future to ion numbers beyond thousands by employing optimized optical fluorescence collection schemes, and later, to observations of emissions going toward the Fock states of indistinguishable photons from atoms inside a cavity [27, 28].

-
- [1] R. J. Glauber, *Physical Review* **131**, 2766 (1963).
 [2] A. Einstein, *Annalen der Physik* **322**, 132 (1905).
 [3] J. C. Maxwell, *Philosophical Transactions of the Royal Society of London* **155**, 459 (1865).
 [4] L. Mandel and E. Wolf, *Optical Coherence and Quantum Optics* (Cambridge University Press, 1995).
 [5] R. J. Glauber, *Quantum Theory of Optical Coherence: Selected Papers and Lectures* (Wiley-VCH, 2007).
 [6] P. K. Tan, G. H. Yeo, H. S. Poh, A. H. Chan, and C. Kurtsiefer, *The Astrophysical Journal Letters* **789**, L10 (2014).
 [7] M. Born and E. Wolf, *Principles of Optics: Electromagnetic Theory of Propagation, Interference and Diffraction of Light* (Cambridge University Press, 2002).
 [8] H. J. Kimble, M. Dagenais, and L. Mandel, *Physical Review Letters* **39**, 691 (1977).
 [9] P. Grangier, G. Roger, and A. Aspect, *Europhysics Letters* **1**, 173 (1986).
 [10] O. A. Shcherbina, G. A. Shcherbina, M. Manceau, S. Vezzoli, L. Carbone, M. De Vittorio, A. Bramati, E. Giacobino, M. V. Chekhova, and G. Leuchs, *Optics Letters* **39**, 1791 (2014).
 [11] L. J. Rogers, K. D. Jahnke, T. Teraji, L. Marseglia, C. Müller, B. Naydenov, H. Schauffert, C. Kranz, J. Isoya, L. P. McGuinness, and F. Jelezko, *Nature Communications* **5**, 4739 (2014).
 [12] L. Lachman, L. Slodička, and R. Filip, *Scientific Reports* **6**, 19760 (2016).
 [13] M. Drewsen, C. Brodersen, L. Hornekær, J. S. Hangst, and J. P. Schiffer, *Physical Review Letters* **81**, 2878 (1998).
 [14] D. B. Higginbottom, L. Slodička, G. Araneda, L. Lachman, R. Filip, M. Hennrich, and R. Blatt, *New Journal of Physics* **18**, 093038 (2016).
 [15] P. Maunz, D. Moehring, S. Olmschenk, K. C. Younge, D. N. Matsukevich, and C. Monroe, *Nature Physics* **3**, 538 (2007).
 [16] C. Kurz, J. Huwer, M. Schug, P. Müller, and J. Eschner, *New Journal of Physics* **15**, 055005 (2013).
 [17] H. G. Barros, A. Stute, T. E. Northup, C. Russo, P. O. Schmidt, and R. Blatt, *New Journal of Physics* **11**, 103004 (2009).
 [18] R. G. Brewer, *Physical Review A* **53**, 2903 (1996).
 [19] R. Short and L. Mandel, *Physical Review Letters* **51**, 384 (1983).
 [20] M. Avenhaus, K. Laiho, M. V. Chekhova, and C. Silberhorn, *Physical Review Letters* **104**, 063602 (2010).
 [21] A. Predojević, M. Ježek, T. Huber, H. Jayakumar, T. Kauten, G. S. Solomon, R. Filip, and G. Weihs, *Optics Express* **22**, 4789 (2014).
 [22] T. E. Northup and R. Blatt, *Nature Photonics* **8**, 356 (2014).
 [23] A. Neuzner, M. Körber, O. Morin, S. Ritter, and G. Rempe, *Nature Photonics* **10**, 303 (2016).
 [24] D. Bhatti, J. Von Zanthier, and G. S. Agarwal, *Scientific Reports* **5**, 17335 (2015).
 [25] F. Jahnke, C. Gies, M. Abmann, M. Bayer, H. Leymann, A. Foerster, J. Wiersig, C. Schneider, M. Kamp, and S. Höfling, *Nature Communications* **7**, 11540 (2016).
 [26] L. Hornekær and M. Drewsen, *Physical Review A* **66**,

013412 (2002).

- [27] B. Casabone, K. Friebe, B. Brandstätter, K. Schüppert, R. Blatt, and T. E. Northup, *Physical Review Letters* **114**, 023602 (2015).
- [28] C. Sayrin, I. Dotsenko, X. Zhou, B. Peaudecerf, T. Rybarczyk, S. Gleyzes, P. Rouchon, M. Mirrahimi, H. Amini, M. Brune, J.-M. Raimond, and S. Haroche, *Nature* **477**, 73 (2011)

Supplementary information: Nonclassical light from large ensemble of trapped ions

A. Experimental setup

Ion trapping

The trap parameters are set with respect to maximizing the stability of particular ion crystal and number of detected photon counts. This corresponds to close to symmetrical configuration of oscillation frequencies of the trapping potential $\omega_x \approx \omega_y \approx \omega_z \approx 778$ kHz for measured ion crystals containing more than 12 ions, and configuration with $\omega_x \approx \omega_y \approx 1341$ kHz and $\omega_z \approx 778$ kHz for measurements with 1 and 12 ions. Here, ω_z is the frequency of the trapping potential in the axial direction of the trap, that is, along the axis connecting the two tip electrodes, and the ω_x, ω_y are the frequencies of the potential in the radial directions which lie in the plane perpendicular to the axial direction. The measured ion ensembles with more than 12 ions correspond to near spherical crystals with concentric shell structure [S1–S3], which have been chosen for optimizing the overall scattered light collection efficiency in the direction perpendicular to the trap axis. The ions are Doppler cooled by red detuned 397 nm laser exciting the $4S_{1/2} \leftrightarrow 4P_{1/2}$ transition and 866 nm laser beam is simultaneously used for repumping the population from the metastable $3D_{3/2}$ state to the cooling transition. The magnetic field of 12 Gauss is applied along the observation direction to lift the degeneracy of the $3D_{3/2}$ state manifold and thus enable its effective depopulation. The excitation beams are co-propagating in the direction perpendicular to magnetic field direction with linear polarization parallel to it.

Light detection

The light scattered from an ensemble of ions is collected by objective covering ~ 2 % of the full solid angle and frequency filtered (IF) to isolate 397 nm fluorescence. The photons are then directed towards one of two possible detection arrangements. The EMCCD camera (Luca-S, Andor) is used for spatial analysis of the trapped ion crystal, estimation of the number of emitters before and after each experimental run, and further calibration measurements, including estimation of the excess micromotion of off-axis positioned ions

and photon emission probability homogeneity across the crystal. The light is further split by beamsplitter (BS) and directed towards a pair of free-space-coupled avalanche photodiodes (APDs, Count-series, Laser Components). The overall detection efficiencies of fluorescence emitted by the ion positioned in the focus of the collection lens has been estimated to be 0.033% and 0.028%, for the APD₁ and APD₂, respectively. Precise arrival times of incoming photons are recorded (PicoHarp300, PicoQuant) with time resolution of 4 ps and further processed to obtain the individual photon detection probabilities. The measured detection efficiencies fall down rapidly for ions displaced radially from the collection objective focal point due to the limited field of view of the whole detection setup, what gives the limit on number of effectively coupled ions. We have separately estimated detection efficiencies for ions displaced in radial and axial direction. In the radial direction of the lens object plane, which corresponds to ion displacement along the trap axis, the measured detection efficiencies of single photon scattered from a single ion normalized to the efficiency in the center yield approximately gaussian efficiency profile with full width at half maximum (FWHM) of 4.6 μm , see Fig. S1. This relatively narrow radial field of view of the employed detection setup is given by the magnification of our detection optics and size of the active detector area. The effective image area is given by the magnification and optical aberrations of the employed optical detection setup consisting of the high-NA objective with object focal distance of approximately 66 mm and additional 400 mm plano-convex lens together with the finite active detection area of the APD of about 100 microns. In the axial direction, the effective ion displacement has been emulated by the collection objective axial displacement using precise translation stage. The measured decrease of the relative detection efficiency is plotted in the fig. A1b. The FWHM of the fitted gaussian function is 238 microns.

Pulsed and continuous modes of excitation

Measurements of nonclassicality of light emitted from ion crystals are realized in both continuous and pulsed regimes, which substantially differ in properties of the emitted light and in the technical feasibility of its detection with the single photon detectors with finite detection bandwidth. We have evaluated this difference by comparison of the $g^2(0) = 0.081$ in the continuous case for a 1 ns time bin and to $g^2(0) = 0.032$ in pulsed excitation.

General remarks

The particular excitation parameters in continuous regime give us at maximum up to 36900 counts/s and 31500 counts/s on APD₁ and APD₂ detectors, respectively, far from the detector saturation rates, which are

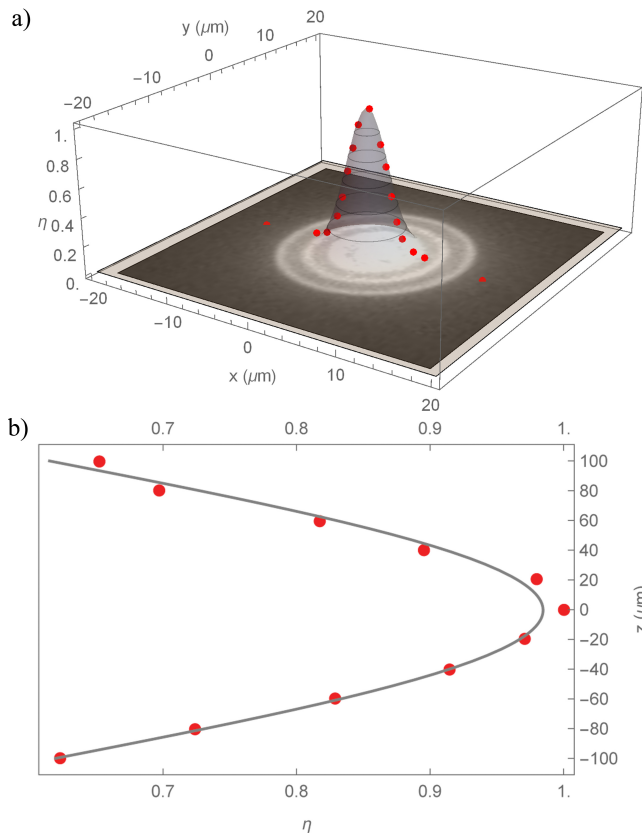


FIG. S1: The measured detection efficiencies in the radial and axial object planes of the employed optical detection system. In a) we plot relative efficiencies normalized to the maximal efficiency corresponding to the lens on-axis position. The bottom plane of the 3D figure is filled with the picture of the ion crystal consisting of $n = 275$ ions scaled to correct units. The graph in b) shows measured efficiencies for the ions effectively displaced along the lens axis for the displacements relevant for the spatial sizes of the measured ion crystals. The fitted Gaussian function has FWHM of 238 microns.

specified to be about in the 10^6 cts/s regime.

B. Data processing

The fluorescence from ion ensemble is detected using two APDs and arrival times of scattered photons are recorded using time-tagged device with 4 ps resolution. Further processing has two parts, manipulation with raw time-tagged data for estimation of probabilities P_{00} and P_0 , and estimation of nonclassicality with corresponding uncertainties. In the first step, we start by evaluation of the total number N_{TB} of all time-bins of size τ in given measurement, N_C number of events where both APDs registered photon in the same time-bin and N_{S1} and N_{S2} , which correspond to events where APD₁ and APD₂ registered the photon, respectively. While in the continuous regime we need to cut the time arrival data

to time-bins, in the pulsed measurements processing is one step easier, because each sequence includes the APD gating pulse which corresponds to single time-bin. We further shorten this time-bin in the data processing step in order to remove the false clicks due to the APD gating pulses, which otherwise correspond to about 10% of real photon detection events depending on the mean input photon flux. According to the employed criterion of non-classicality, we need to estimate the probabilities P_{00} and P_0 . The measured photon detection numbers are related to these probabilities through following relationships:

$$P_{00} = \frac{N_{\text{TB}} - N_{S1} - N_{S2} - N_C}{N_{\text{TB}}}, \quad (\text{S1})$$

$$P_{0k} = \frac{N_{\text{TB}} - N_{S_k} - N_C}{N_{\text{TB}}} \quad (\text{S2})$$

and

$$P_0 = \sqrt{P_{01} \cdot P_{02}}, \quad (\text{S3})$$

where the use of the geometrical mean is due to slight imbalance between the absolute detection efficiencies in our detection apparatus. The use of the geometrical mean here is justified by following consideration. For a known unbalancement T of the detection efficiencies, nonclassicality is witnessed if at least one of the following conditions is satisfied [S4]

$$P_{01} > P_{00}^T, \quad (\text{S4})$$

$$P_{02} > P_{00}^{1-T}. \quad (\text{S5})$$

Multiplying left and right sides of those inequations excludes T and leads directly to

$$P_{01} \cdot P_{02} > P_{00}. \quad (\text{S6})$$

It is obvious, that if this relation holds, at least one of inequations has to be satisfied, which guarantees the non-classicality.

From P_0 and P_{00} we estimate nonclassicality of the measured light field using the equation (1) from the main part of the manuscript. The error bars are estimated statistically by dividing our 5 hour long measurement to 5 parts of equal length for which the nonclassicality has been estimated independently.

C. Simulations

Estimation of the theoretical distance for our experimental setup

Although the source of light consisting of trapped ions is very complex system with large number of inner parameters, one can capture the properties of the emerging light using several simplifying assumptions about the

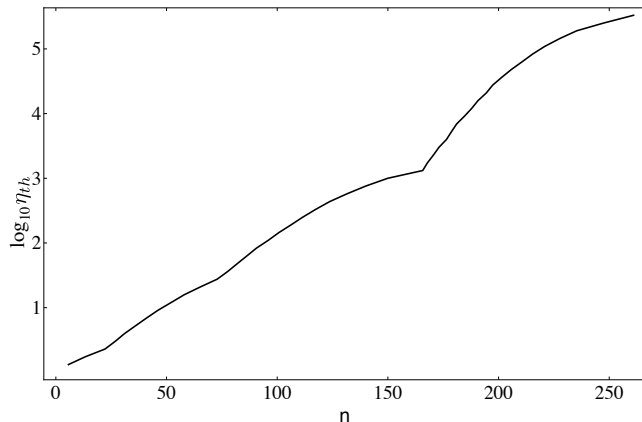


FIG. S2: Simulation of number of contributing emitters n with the efficiency higher than relative threshold efficiency $\eta_{\text{th}} = \eta_0/\eta$.

physics behind. First, each ion is treated as an ideal single photon emitter whose emission is independent on the presence or state of other ions. This means that the light is radiated independently. The cooling of the ions causes formation of the ion crystal. The crystal in our measurement has spherical symmetry (except the crystal with 12 ions) and a shell structure. The numbers of ions in different shells are obtainable by simulation of molecular dynamics [S5]. The occupation of shells in our crystals is following, crystal with 12 ions is formed only in one shell, crystal with 55 ions has two shells (12+43 ions), crystal with 125 ions has three shells (82+35+8 ions), crystal having 204 ions consists of four shells (115+60+25+4 ions), crystal with 275 has also four shells (150+80+36+9 ions). According to the numerical model from [S5], the spacing among particular shells is almost constant. Additionally, we suppose that ions within shells have no crystal structure but rather correspond to a gaseous or plasma state with homogeneous but random distribution in each shell [S1, S3, S5]. This assumption is supported by our measurements of ion ensemble images on EMCCD camera. To simulate this random distribution, we choose several polyhedra carrying some symmetry whose vertices after random rotation determine the position of ions on a shell. Therefore the simulation requires sufficient number of random rotations of each polyhedron to obtain homogenous distribution of vertices. The employed polyhedra are tetrahedron (four vertices), cube (8 vertices), regular icosahedron (12 vertices), regular dodecahedron (20 vertices) and truncated icosahedron (60 vertices). To simulate a shell with arbitrary number of ions, we can combine these polyhedrons and randomly delete a few vertices to adjust the total vertices to the desired number.

If the ions are excited, they act as single photon emitters radiating photons by spontaneous emission to directions defined by given dipole radiation pattern. How-

ever, the lens is able to collect and focus on detectors only a small part of this emission. This, together with quantum efficiency of detectors, yields overall detection efficiency $\eta_0 = 6.1 \cdot 10^{-4}$ for the emitters situated in the object focal point of the whole detection optical setup. As demonstrated in measurements presented in Supplementary information A, emitters positioned out of the focus are observed less likely due to decreased detection efficiency. We assume that the detection efficiency depends on position as

$$\eta = \eta_0 \cdot e^{-\frac{r^2}{2\sigma_r^2} - \frac{a^2}{2\sigma_a^2}} \quad (\text{S7})$$

where r is the distance from the optical axis of the lens and a is the distance from the focal plane. σ_r and σ_a correspond to variances of this Gaussian distribution. We have experimentally estimated their values $\sigma_r = 2.3 \mu\text{m}$ and $\sigma_a = 98 \mu\text{m}$. It suffices to use only one crystal for the calibration of the spatial size in the simulation, because the ratio of number of ions in a crystal and its volume is approximately constant [S5]. This approach significantly assigns statistics of detector clicks to a crystal having n ions. The probabilities P_{00} , P_0 employed in our criterion of nonclassicality are obtained by $P_{00} = \prod_{i=1}^n (1 - \eta_i)$ and $P_0 = \prod_{i=1}^n (1 - \eta_i/2)$. This enables to plot the estimate of parameter d for crystals in our measurement as depicted in Fig. 2 in the main part of the manuscript. The largest crystal in these measurements contained $n = 275$ ions. However, as described in the supplementary information A, not all emitters contributed equally to the detected light. The measured detection efficiencies as a function of radial ion displacement show, that increase of the measured crystal size beyond approximately hundred ions inevitably places some of them into the regions with very small relative detection efficiency. This gives raise to a questions about the lowest detection efficiency of ion, which is still relevant for the observed light statistics, relative to the ion with maximal detection efficiency. Because it cannot be answered generally, we estimate the number of ions from which photons are detected with probability above some value, see Fig. S2. Apparently, the narrow volume of the lens significantly suppresses detection of photons emitted from outer shelves of the crystal.

Prospect of measurements on higher number of trapped ions

The theoretical prediction of visibility of nonclassicality for higher photon flux requires both the estimation of the parameter d and corresponding uncertainty that stems from fluctuation of experimental outputs (S1) and (S2). Let us introduce a linear combination of the measured quantities and their mean values

$$\begin{aligned} X &= 2P_0 - P_{00} \\ Y &= P_0 + 2P_{00} \\ x &= \langle X \rangle \\ y &= \langle Y \rangle. \end{aligned} \quad (\text{S8})$$

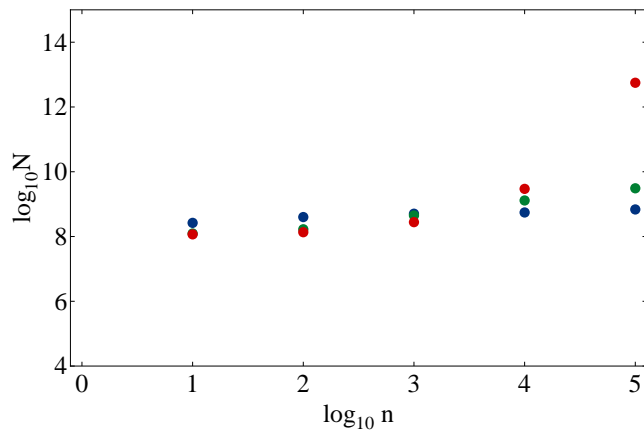


FIG. S3: The number N of experimental runs necessary to violate the nonclassicality by two errorbars is depicted for crystals counting n ions. The parameters of the detection are $\eta = 4 \times 10^{-4}$ and $\sigma_a = 98 \mu\text{m}$. Different colors correspond to $\sigma_r = 2 \mu\text{m}$ (blue), $\sigma_r = 8 \mu\text{m}$ (green) and $\sigma_r = 20 \mu\text{m}$ (red).

The density probability function of random quantities X and Y is approximated in the limit of a high number of experimental runs by Gaussian distribution

$$P(X, Y) = \frac{1}{2\pi\sqrt{V_x V_y}} \exp\left[-\frac{(X-x)^2}{2V_x} - \frac{(Y-y)^2}{2V_y}\right], \quad (\text{S9})$$

where $V_{x,y}$ is the variance of the variable X, Y . These quantities are related to detection events such that

$$\begin{aligned} \langle X \rangle &= 1 - P_c \\ \langle Y \rangle &= \frac{1}{2}P_s + \frac{3}{2}P_{00}, \end{aligned} \quad (\text{S10})$$

where P_c is a probability of a coincidence click and P_s means probability of just a single click. Thus, the variances obey

$$\begin{aligned} V_x &= \frac{P_c(1 - P_c)}{N} \\ V_y &= \frac{P_s(1 - P_s)}{4N} + \frac{9P_{00}(1 - P_{00})}{4N}. \end{aligned} \quad (\text{S11})$$

The parameter d is given by

$$d = \frac{2X + Y}{5} - \sqrt{\frac{-X + 2Y}{5}}. \quad (\text{S12})$$

The density probability function (S9) enables to obtain

$$\text{var}(d) = V_x \left(\frac{\sin \phi}{2\sqrt{P_{00}}} + \cos \phi \right)^2 + V_y \left(\frac{\cos \phi}{2\sqrt{P_{00}}} - \sin \phi \right)^2, \quad (\text{S13})$$

where $\phi = \arctan 1/2$. For very weak light source, one gets $\text{var}(d) \approx 0.315P_c/N \ll \text{var}(P_0)$, which indicates that the measured point fluctuates mainly in direction parallel with the curve corresponding to nonclassicality threshold.

The shell structure of a crystal simulated in [S5] is presented completely for crystals containing up to 2000 ions. Crystal with higher number of ions tend to change the arrangement of ions to bcc grid [S6]. The Cartesian coordinates of emitters in the bcc grid are given by formulas

$$\begin{aligned} x_i &= iu + \frac{1}{4} [-(-1)^j + 1] u \\ y_j &= j \frac{\sqrt{3}}{2} u + \frac{1}{2\sqrt{3}} u [-(-1)^k + 1] \\ z_k &= k \sqrt{\frac{2}{3}} u, \end{aligned} \quad (\text{S14})$$

where u is a distance between two ions and i, j and k are integers. To emphasize further scalability of our measurements, we analyze number of experimental runs necessary for violation of nonclassicality by two standard deviations, see Fig. S3.

[S1] M. Drewsen, C. Brodersen, L. Hornekær, J. S. Hangst, and J. P. Schiffrer, *Physical Review Letters* **81**, 2878 (1998).

[S2] L. Hornekær and M. Drewsen, *Physical Review A* **66**, 013412 (2002).

[S3] K. Okada, M. Wada, T. Takayanagi, S. Ohtani, and H. A. Schuessler, *Physical Review A* **81**, 013420 (2010).

[S4] R. Filip and L. Lachman, *Physical Review A* **88**, 043827 (2013).

[S5] R. W. Hasse and V. V. Avilov, *Physical Review A* **44**, 4506 (1991).

[S6] H. Totsuji, T. Kishimoto, C. Totsuji, and K. Tsuruta, *Physical Review Letters* **88**, 125002 (2002)